Journal of Sound and Vibration (2002) **256**(5), 941–954
doi:10.1006/jsvi.5027, available online at http://www.idealibrary.com on IDEAL®

APPROXIMATE TRANSMISSION EQUIVALENCE OF ELASTIC BAR TRANSITIONS UNDER 3-D CONDITIONS

B. LUNDBERG

The Ångström Laboratory, Uppsala University, Box 534, *SE*-751 21 *Uppsala, Sweden.*
E-mail: bengt.lundberg@angstrom.uu.se

AND

M. OKROUHLIK

Institute of Thermomechanics, Dolejskova 5, *CZ*-182 00 *Prague, Czech Republic. E-mail: ok@it.cas.cz*

(*Received* 25 *June* 2001, *and in final form* 7 *December* 2001)

Transmission of quasi-longitudinal elastic waves through elastic bar transitions between uniform and collinear bar segments is studied by means of three-dimensional (3-D) finite element analysis. The aim is to examine, through an example, to what extent two geometrically different transitions which are transmission-equivalent in a one-dimensional (1-D) context may retain this property under 3-D conditions. The difference between the two transitions is assessed from the difference between 3-D results for reflected waves, while the presence of 3-D effects is judged from the difference between 3-D finite element and 1-D analytical results for transmitted waves. It is found that two smooth and significantly different elastic bar transitions which are transmission-equivalent in a 1-D context may retain this property with good approximation under significantly 3-D conditions, well beyond those under which 1-D theory can be used for prediction of wave shapes. This extends the domain of potential applications in areas such as percussive drilling correspondingly.

1. INTRODUCTION

The ability of elastic waves to transport and deliver energy has important applications in engineering. In percussive drilling of rock [1], for example, this ability is used to transmit energy through a drill string to a drill bit which converts a substantial part of the wave energy into work when it crushes the rock. Normally, there are changes in cross-sectional area along the drill string, corresponding to transitions in characteristic impedance, which may significantly affect the transmission as well as the conversion of energy.

A quasi-longitudinal elastic wave travelling through a straight and uniform segment of an elastic bar is transmitted without reduction of its energy due to reflection. If the dominating wavelengths are long compared with the lateral dimensions of the bar, so that approximate one-dimensional (1-D) conditions prevail, the wave is also transmitted without significant distortion of its shape due to dispersion [2]. When, in contrast, a wave is transmitted from one uniform segment of a bar to another through a transition with changing material or lateral dimensions, reflection normally occurs so that the wave is transmitted with a reduction of its energy and a change of its length and shape. In engineering applications, such changes may have significant effects on efficiencies and other measures of performance.

0022-460X/02/$35.00

There has long been interest in the transmission of waves through elastic bar transitions [3, 4] and in maximizing efficiency of energy transmission by optimizing either the shape of the incident wave [5] or that of the transition itself [6–8]. Interest has also been devoted to similar problems for viscoelastic bar transitions [9, 10].

This paper deals with the transmission of quasi-longitudinal elastic waves through transitions between uniform and collinear bar segments with given characteristic impedances. More specifically, the interest concerns bar transitions made of the same elastic material which are significantly different from each other in terms of geometry, mass and reflection properties but yet have the same or approximately the same transmission properties. For the same arbitrary incident wave, such transitions produce transmitted waves which are the same, or approximately the same. This means, for example, that corresponding stress components associated with two such transmitted waves, and their distributions in space and time, should be the same or approximately the same.

In a 1-D context, there generally exist transitions which are transmission equivalent, in an exact sense, to a given transition [4]. For a given transition which consists of a finite number N of segments with constant characteristic impedances and equal transit times, there are at most 2^N such transitions, including the one given. They can be obtained systematically through inversion in the unit circle of zeroes of a polynomial of degree N [4, 11], which characterizes the given transition. One of these transitions, which corresponds to the inversion of all such zeroes, can also be constructed through combined inversion and reversion of the characteristic impedance function of the given transition. For equal input and output characteristic impedances, two of the transmission-equivalent transitions can also be obtained by inversion alone or, due to reciprocity [12–14], by reversion alone. It should be noted that although two transmission-equivalent transitions with different distributions of characteristic impedance have the same transmission properties, they do not have the same reflection properties.

In exceptional cases it may occur that a given transition does not have any transmission-equivalent transition different from itself. This is the situation for a transition which is optimal in the sense that it maximizes the energy transmission for some incident wave. Such a transition has all zeroes of its characteristic polynomial on the unit circle, and therefore inversions of zeroes or corresponding transformations of the characteristic impedance function, do not produce new transitions [4].

The existence, in general, of bar transitions which are transmission equivalent to one which is given has potential use in engineering applications such as percussive drilling of rock. For example, it may be interesting to redesign a bar transition in order to reduce its mass, increase its strength or simplify its production without changing its transmission properties. An attractive way to do this would be to make a suitable choice among all bar transitions which have the same transmission properties as the original one.

The aim of this paper is to examine, through an example, to what extent two geometrically different bar transitions which are transmission equivalent in a 1-D context may retain this property under three-dimensional (3-D) conditions. The first bar transition to be considered will have conical shape and a corresponding distribution of its characteristic impedance. The shape of the second will correspond to a characteristic impedance function which results from combined inversion and reversion of that of the first.

In section 2, the 1-D distribution of axial stress in the output segments of the two bars will be determined for a given input. As transmission equivalence is exact in the 1-D context, it will suffice to consider the bar with a conical transition. In section 3, axisymmetric finite element analyses will be carried out in order to obtain the corresponding 3-D distributions of axial normal stress on the axes and surfaces of the two bars. In sections 4 and 5, the difference between the two bar transitions will be assessed from the difference between the

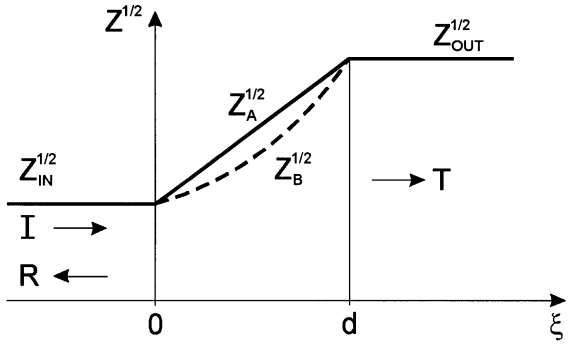

Figure 1. Transmission-equivalent pair of elastic bar transitions with variable characteristic impedances $Z_A(\xi)$ and $Z_B(\xi)$ between input and output bar segments with constant characteristic impedances Z_{IN} and Z_{OUT}. The characteristic impedance $Z_B(\xi)$ is obtained through combined inversion and reversion of the characteristic impedance function $Z_A(\xi)$.

3-D results for reflected waves, while the presence of 3-D effects will be judged from the difference between the 3-D finite element and the 1-D analytical results for transmitted waves. Finally, comparison of the 3-D results for transmitted waves will show to what extent the property of transmission equivalence in a 1-D context is retained under 3-D conditions.

2. ONE-DIMENSIONAL ANALYSIS

Consider propagation of quasi-longitudinal elastic waves under 1-D conditions in a straight bar with cross-sectional area A, Young's modulus E and density ρ. Generally, these quantities, the wave speed $c = (E/\rho)^{1/2}$ and the characteristic impedance $Z = AE/c$ may depend on the axial co-ordinate x. With the introduction of the characteristic impedance function $Z(\xi)$, where $\xi = \int_0^x \mathrm{d}s/c(s)$ is a transformed axial co-ordinate which expresses the travel time from the origin to x, the propagation of waves in the bar is modelled by the relations

$$\frac{\partial N}{\partial \xi} = Z\frac{\partial v}{\partial t}, \qquad \frac{\partial v}{\partial \xi} = \frac{1}{Z}\frac{\partial N}{\partial t}, \tag{1}$$

which originate from the equation of axial motion and Hooke's law respectively. In these relations, $N(\xi, t) = Z\partial u/\partial \xi$ is the normal force, $v(\xi, t) = \partial u/\partial t$ is the particle velocity and $u(\xi, t)$ is the displacement, positive in the direction of increasing ξ. In what follows, it will be assumed that Young's modulus E and the density ρ are constant, so that variations in the characteristic impedance $Z(\xi)$ are due entirely to corresponding variations in the cross-sectional area $A(\xi)$.

Let the input segment $\xi < 0$ of the bar have the constant characteristic impedance $Z(\xi) = Z_{IN}$, and let the output segment $\xi > d$ have the constant characteristic impedance $Z(\xi) = Z_{OUT}$ as shown in Figure 1. Then, equations (1) result in the wave equation for N and v in these parts of the bar, and the distributions of normal force and particle velocity become

$$N(\xi, t) = N_I(t - \xi) + N_R(t + \xi), \qquad v(\xi, t) = \frac{1}{Z_{IN}}[-N_I(t - \xi) + N_R(t + \xi)] \tag{2}$$

in the input segment and

$$N(\xi, t) = N_T(t - \xi), \qquad v(\xi, t) = \frac{1}{Z_{OUT}} N_T(t - \xi) \tag{3}$$

in the output segment. The functions $N_I(t)$, $N_R(t)$ and $N_T(t)$ represent the incident, reflected and transmitted waves, respectively, and use has been made of the circumstance that there is no wave incident on the transition from the right. The corresponding distributions of normal stress can be obtained as $\sigma = N/A_{IN}$ and N/A_{OUT} respectively.

Furthermore, let one transition $0 \leqslant \xi \leqslant d$, labelled A, be conical and have the characteristic impedance

$$Z_A(\xi) = C(a + \xi)^2, \tag{4}$$

where C and a are parameters such that $Z_A(0) = Z_{IN}$ and $Z_A(d) = Z_{OUT}$. Corresponding to this transition, there is another transition, labelled B, with characteristic impedance

$$Z_B(\xi) = Z_{IN}Z_{OUT}/C(a + d - \xi)^2 \tag{5}$$

and transmission properties identical to those of transition A [4, 12]. This transition is obtained through combined inversion (replacement of $Z_A(\xi)$ by $Z_{IN}Z_{OUT}/Z_A(\xi)$) and reversion (replacement of $Z_A(\xi)$ by $Z_A(d - \xi)$) of the characteristic impedance function (4) of transition A, that is, through the transformation $Z_B(\xi) = Z_{IN}Z_{OUT}/Z_A(d - \xi)$. Similar to transition A, transition B has the properties $Z_B(0) = Z_{IN}$ and $Z_B(d) = Z_{OUT}$. Otherwise, the two transitions are different provided that $Z_{IN} \neq Z_{OUT}$. They are illustrated in Figure 1.

Next, the aim is to determine, for both transitions, the transmitted wave produced by a given incident wave. As the transmission properties of the two transitions are identical, it will be sufficient to consider transition A in what follows. For this transition, equations (1) and (4) give the wave equation for the product $(a + \xi)v(\xi, t)$. From its solution, the distributions of normal force and particle velocity in the transition are obtained as

$$N(\xi, t) = \frac{Z_A(\xi)}{a + \xi}[-p'(t - \xi) + n'(t + \xi)] - \frac{Z_A(\xi)}{(a + \xi)^2}[p(t - \xi) + n(t + \xi)],$$

$$v(\xi, t) = \frac{1}{a + \xi}[p'(t - \xi) + n'(t + \xi)], \tag{6}$$

where p and n are functions which represent waves travelling in the directions of increasing and decreasing ξ respectively. The prime symbol indicates differentiation with respect to the arguments $t \pm \xi$ of these functions.

Equations (2), (3) and (6), and the requirement of continuity of normal force and particle velocity at the ends of the transition, provide a system of four difference–differential equations which relate the four unknown functions $p(t)$, $n(t)$, $N_R(t)$ and $N_T(t)$. From this system, and the requirement that the functions $p(t)$ and $n(t)$ be continuous with $p(t) = 0$ for $t < 0$ and $n(t) = 0$ for $t < 2d$, the unknown functions can be determined successively in the intervals $0 \leqslant t < 2d$, $2d \leqslant t < 4d$, … . For $t < 0$, these functions are zero.

The incident wave is defined by the rectangular compressive pulse

$$N_I(t) = -N_0[\mathrm{H}(t) - \mathrm{H}(t - \lambda)], \tag{7}$$

where N_0 is the amplitude, λ is the duration and $\mathrm{H}(t)$ is Heaviside's unit step function. The front of the wave arrives at the input end of the transition at time $t = 0$. As only relatively short incident pulses with $\lambda \leqslant 2d$ are of interest, it is sufficient to determine $N_R(t)$ and $N_T(t)$

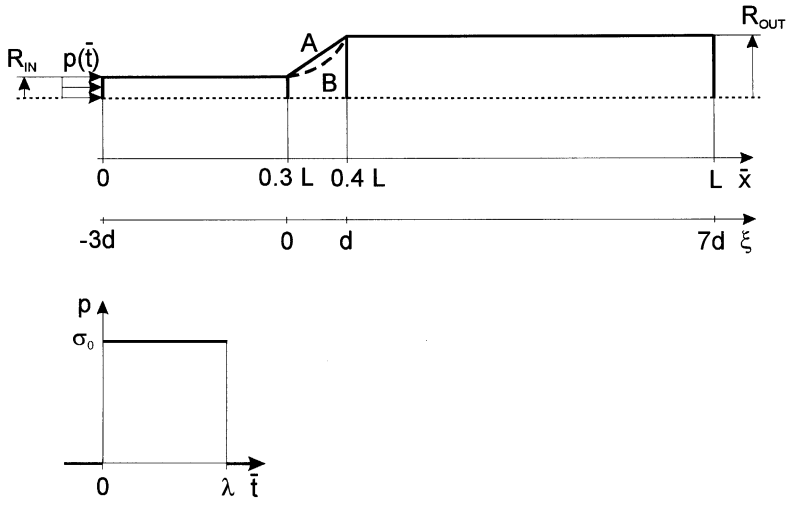

Figure 2. Transmission-equivalent pair of elastic bar transitions A and B between pressure-loaded input bar segment with diameter D_{IN} and free-ended output bar segment with diameter D_{OUT}. The shape of B is obtained through combined inversion and reversion of the characteristic impedance function of A.

in the interval $0 \leqslant t < 2d$. The result is

$$N_R(t) = -N_0[f_R(t) - f_R(t-\lambda)], \quad f_R(t) = (1 - e^{-\alpha t})H(t) \tag{8}$$

and

$$N_T(t) = -N_0[f_T(t) - f_T(t-\lambda)], \quad f_T(t) = \frac{r}{r+1}(re^{-\alpha t} + e^{\beta t})H(t), \tag{9}$$

where

$$r = (Z_{OUT}/Z_{IN})^{1/2}, \qquad \alpha = (r-1)\frac{1}{2d}, \qquad \beta = \frac{(r-1)}{r}\frac{1}{2d}. \tag{10}$$

Although transitions A and B have the same transmission properties, they do not have the same reflection properties. Therefore, while the transmitted wave defined by equations (9) is valid for both transitions A and B, the reflected wave defined by equations (8) is valid for transition A only. It is also noted that r is equal to the diameter ratio D_{OUT}/D_{IN} if the material is the same in the input and output segments.

3. THREE-DIMENSIONAL ANALYSIS

3.1. GEOMETRY, MATERIAL AND LOAD

Bars A and B shown in Figure 2 were considered for the 3-D finite element analysis. They have circular cross-sections, input diameter $2R_{IN} = D_{IN} = 20$ mm, output diameter $2R_{OUT} = D_{OUT} = 3D_{IN} = 60$ mm, length of transition $L_{TR} = 5D_{IN} = 100$ mm and total length $L = 10L_{TR} = 1000$ mm. The material is steel with the Poisson ratio $\nu = 0{\cdot}3$, Young's modulus $E = 210$ GPa, density $\rho = 7800\,\text{kg/m}^3$ and 1-D wave speed $c = (E/\rho)^{1/2} = 5189$ m/s.

The ends of the input segments are located at $\bar{x} = 0$, the transitions at $0.3L \leqslant \bar{x} \leqslant 0.4L$, and the ends of the output segments at $\bar{x} = L$. Here, $\bar{x}$ is an axial co-ordinate which is

related to those introduced previously through $\bar{x} = 0{\cdot}3L + x = 0{\cdot}3L + c\xi$. Transition A is conical with radius $R_A(x)$, while B has a radius $R_B(x)$ which approximates $R_{IN}R_{OUT}/R_A(0{\cdot}1L - x)$ with a piece-wise linear function. The approximation is such that equality prevails at five (coarse mesh) or seven (fine mesh) equidistant points, including the ends of the transition.

The input ends of the bars are loaded with a rectangular pressure pulse $p(\bar{t})$ with duration $\lambda = 0{\cdot}5d$, d and $2d$, and amplitude $\sigma_0 = N_0/A_{IN} = 405$ MPa as shown in Figure 2, while the output ends are free. Here $d = L_{TR}/c = 0{\cdot}1L/c$ is the transit time for a 1-D wave through the transitions. The time $\bar{t}$ is shifted relative to t so that $\bar{t} = 3d + t$.

3.2. DIMENSIONLESS PARAMETERS AND VARIABLES

The significant parameters of the problem are the dimensionless ones which define the shape of the transitions ($D_{OUT}/D_{IN} = 3$ and $L_{TR}/D_{IN} = 5$), the material ($\nu = 0{\cdot}3$) and the duration of the pressure pulse relative to the transit time through the transition ($\lambda/d = 0{\cdot}5$, 1 and 2). The dimensional input parameters for the finite element analyses given above are used for convenience. The ratio $L/L_{TR} = 10$ is slightly larger than that needed to prevent reflected waves from the bar ends from overlapping the transmitted wave during the period of time $0 \leqslant t \leqslant 5{\cdot}33d$ considered. Otherwise, this parameter is not significant.

As the problem considered is linear, the axial normal stress in the bar σ is directly proportional to the amplitude σ_0 of the applied pressure and thus σ/σ_0 is independent of σ_0. Therefore, the results of the analyses will be presented as dimensionless axial normal stress σ/σ_0 versus dimensionless position ξ/d at a fix dimensionless time t/d.

The above choice of dimensionless parameters has been made with the purpose that (i) the bar transitions A and B should be significantly different from each other and (ii) 3-D effects should be important. It can be shown that in terms of these parameters the ratio of the masses of these transitions is

$$M_A/M_B = (D_{OUT}/D_{IN} + 1 + D_{IN}/D_{OUT})/3, \tag{11}$$

which gives $M_A/M_B = 1{\cdot}44$. Thus, the mass of transition A is 44% larger than that of transition B. The significance of 3-D effects can be assessed in terms of the ratio of pulse length to output diameter, which is estimated to be of the order of unity for the shortest pressure pulse. Therefore, the dominating wavelengths are comparable with the transverse dimensions of the bars and 3-D effects are expected to be significant [2].

3.3. FINITE ELEMENT ANALYSIS

Marc, a general-purpose finite element code from MSC Software Corporation, was employed for the 3-D finite element analysis, and pre- and post-processing were carried out with Matlab. A four-node axisymmetric element with a fully integrated bilinear shape function was used to obtain the stiffness and mass matrices. Consistent mass matrix formulation together with the implicit Newmark time operator with $\gamma_{Newmark} = 0{\cdot}5$ (no numerical damping) were employed. With this choice [15, 16], the dispersive errors due to the time and space discretization are of opposite signs. Spatial discretization side effects were reduced also by using a nearly uniform mesh.

In order to capture high-frequency components of the rectangular input pulse, use was made of a time step h, corresponding to the highest frequency of the finite element structure. A suitable time step was estimated by relating it to the time $t_{MIN} = l_{MIN}/c'$ needed for a wave

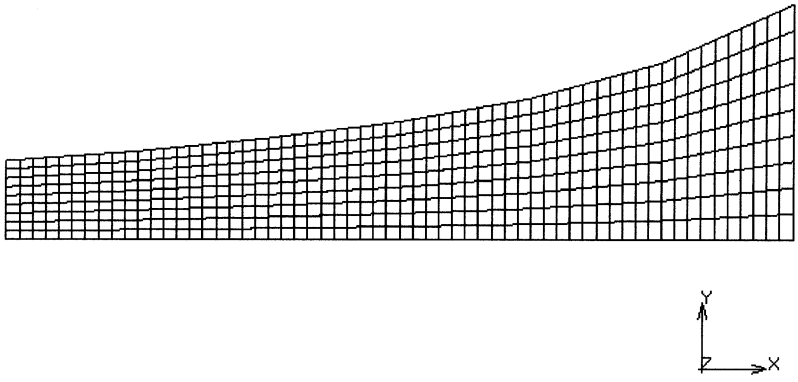

Figure 3. Finite element meshes for bars with transmission-equivalent pair of transitions A and B.

front to pass through a characteristic length l_{MIN} of the smallest element of the structure with a characteristic wave speed c'. Here, $c' = c = (E/\rho)^{1/2}$ was a natural choice. In this way, the time step $h = t_{MIN}/2$ was found to provide a suitable trade-off between minimization of time dispersion errors and demand of CPU time.

Space discretization considerations demand at least five elements within a wavelength in order that a harmonic be captured with an error less than 1%. Requirement to register frequencies up to at least 1 MHz and wave speed of about 5000 m/s led to an element size of the order of 1 mm, see references [16, 17].

Two finite element meshes were used for each transition, one fine and one coarse. The fine meshes involved 600 elements axially and nine elements axially throughout the bars, that is, altogether 5400 elements. With this choice, the elements in the input segment were rectangular with axial and radial dimensions 1·67 and 1·11 mm, respectively, while those in the output segment were rectangular with length 1·67 mm and height 3·33 mm. The coarse meshes, involving 2700 elements, were obtained by reducing to half the number of elements axially. The transition parts of the fine meshes are illustrated in Figure 3.

4. RESULTS

The influence of mesh size on the 3-D distribution of axial normal stress at time $t = 5{\cdot}33d$ is shown in Figure 4 for the bar with transition A and in Figure 5 for that with transition B. In both cases, the incident wave is generated by a rectangular pressure pulse with duration $\lambda = 0{\cdot}5d$.

The 3-D distributions of axial normal stress at time $t = 5{\cdot}33d$ on the surfaces and on the axes of the two bars, one with transition A and one with transition B, are shown in Figure 6. The corresponding 1-D distribution of normal stress in the output segments of the two bars, exactly the same for transitions A and B, is also shown. In both cases, the incident wave is generated by a rectangular pressure pulse with duration $\lambda = 0{\cdot}5d$, and use is made of the fine mesh. Corresponding results obtained with the coarse mesh are shown in Figure 7 for $\lambda = d$ and in Figure 8 for $\lambda = 2d$.

5. DISCUSSION

At time $t = 5{\cdot}33d$, which corresponds to the stress distributions shown in Figures 4–8, the fronts of the 1-D transmitted waves have reached $\xi = 5{\cdot}33d$ in the output segments, while

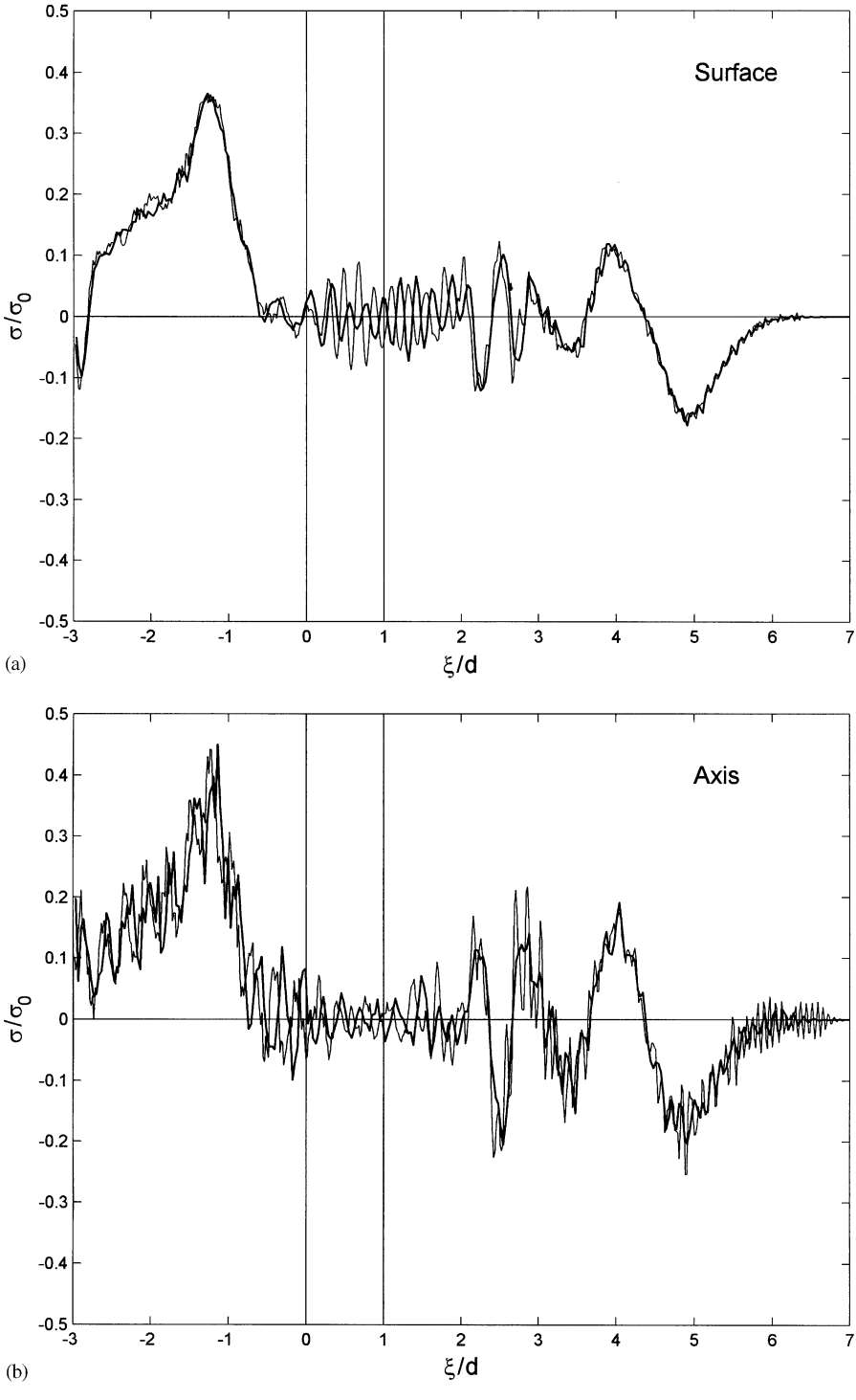

Figure 4. 3-D distribution of axial normal stress at time $t = 5.33d$ in bar with transition A for fine (thin curve) and coarse (thick curve) meshes. Ends of transition indicated by vertical lines. Duration of input pressure pulse $\lambda = 0{\cdot}5d$. (a) Surface. (b) Axis.

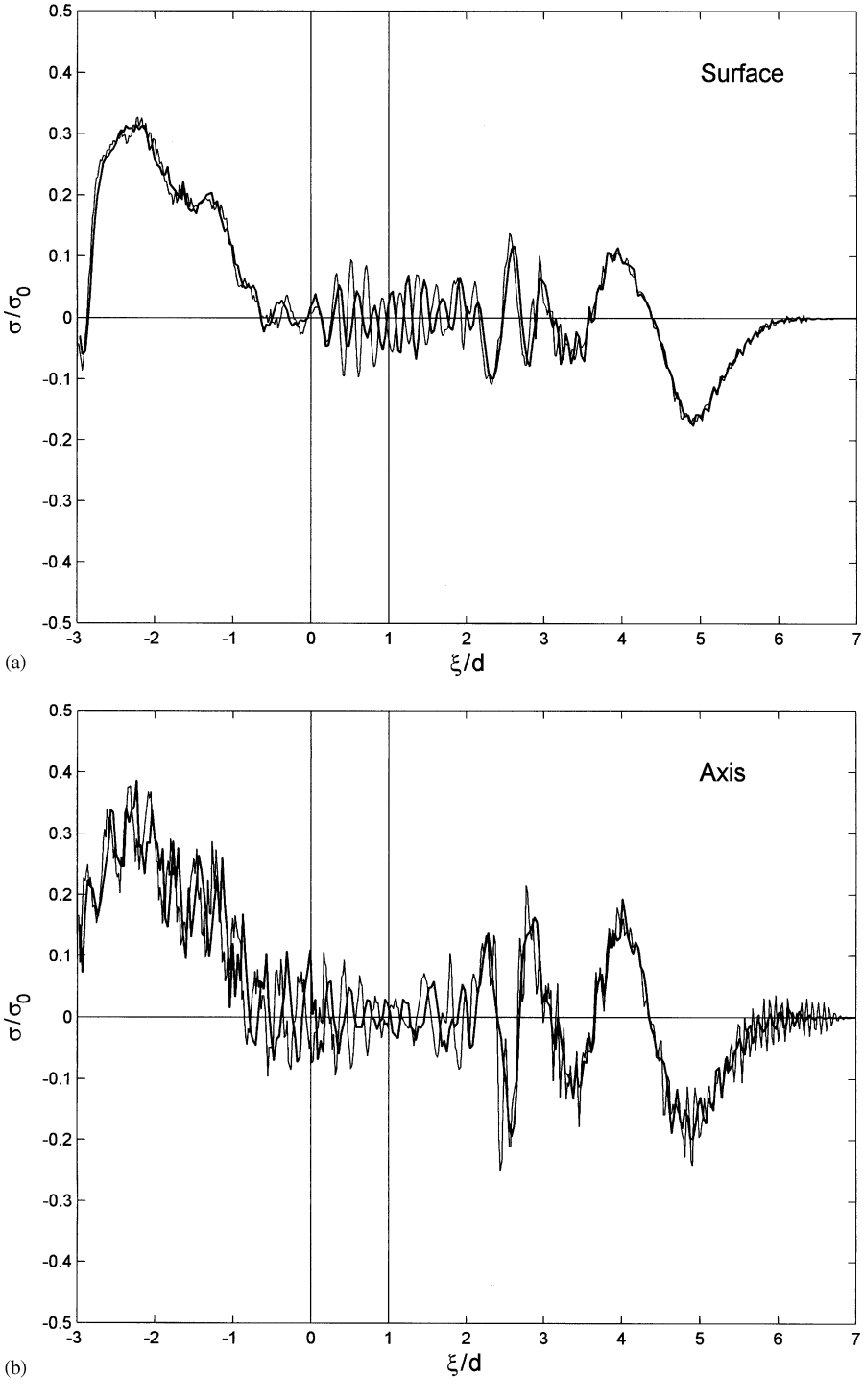

Figure 5. 3-D distribution of axial normal stress at time $t = 5.33d$ in bar with transition B for fine (thin curve) and coarse (thick curve) meshes. Ends of transition indicated by vertical lines. Duration of input pressure pulse $\lambda = 0{\cdot}5d$. (a) Surface. (b) Axis.

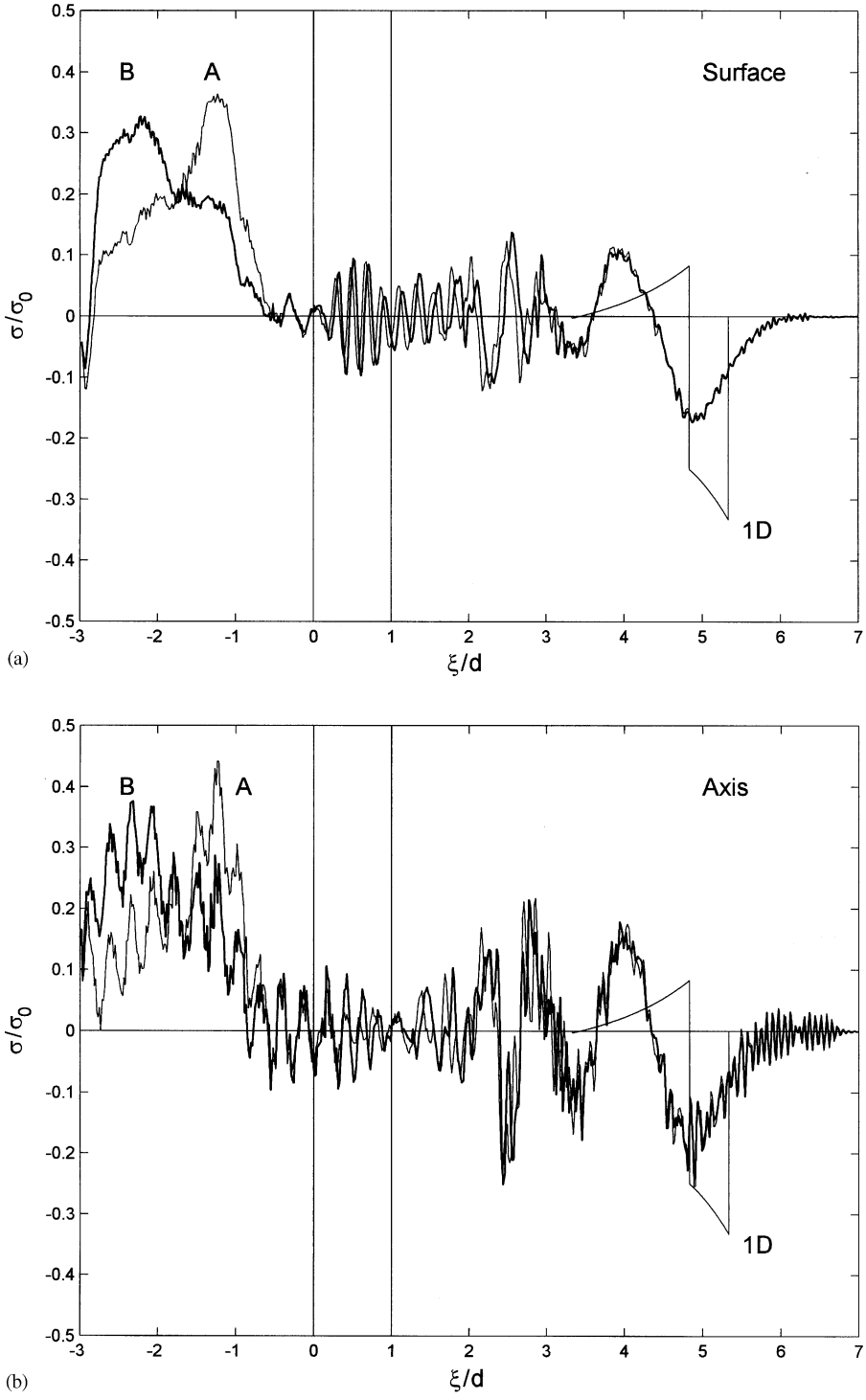

Figure 6. 3-D and 1-D distributions of axial normal stress at time $t = 5{\cdot}33d$ in bars with transitions A and B. Ends of transition indicated by vertical lines. Duration of input pressure pulse $\lambda = 0{\cdot}5d$. Fine mesh. (a) Surface. (b) Axis.

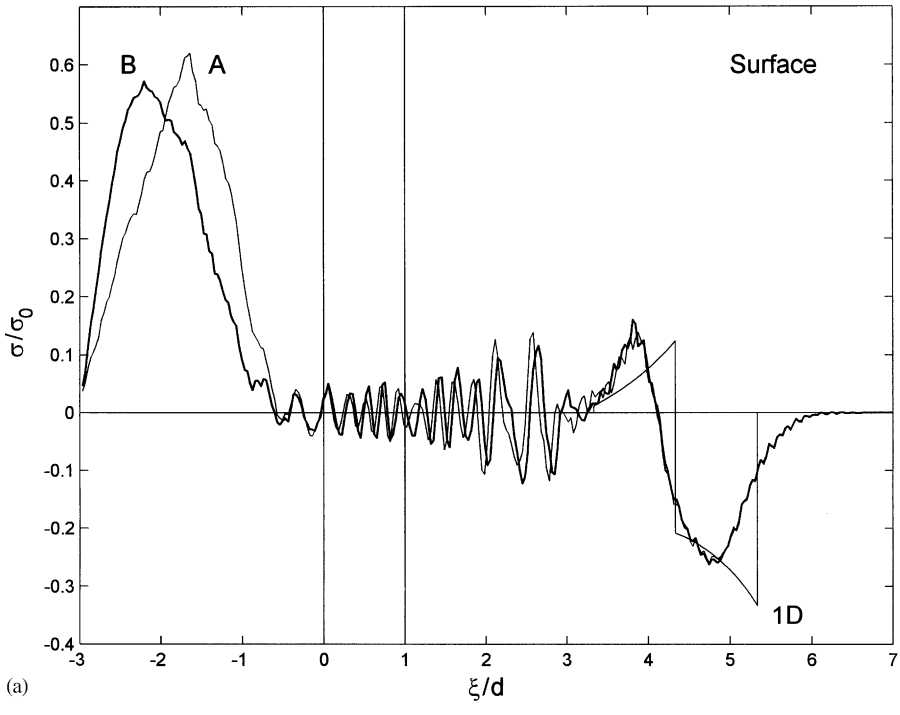

(a)

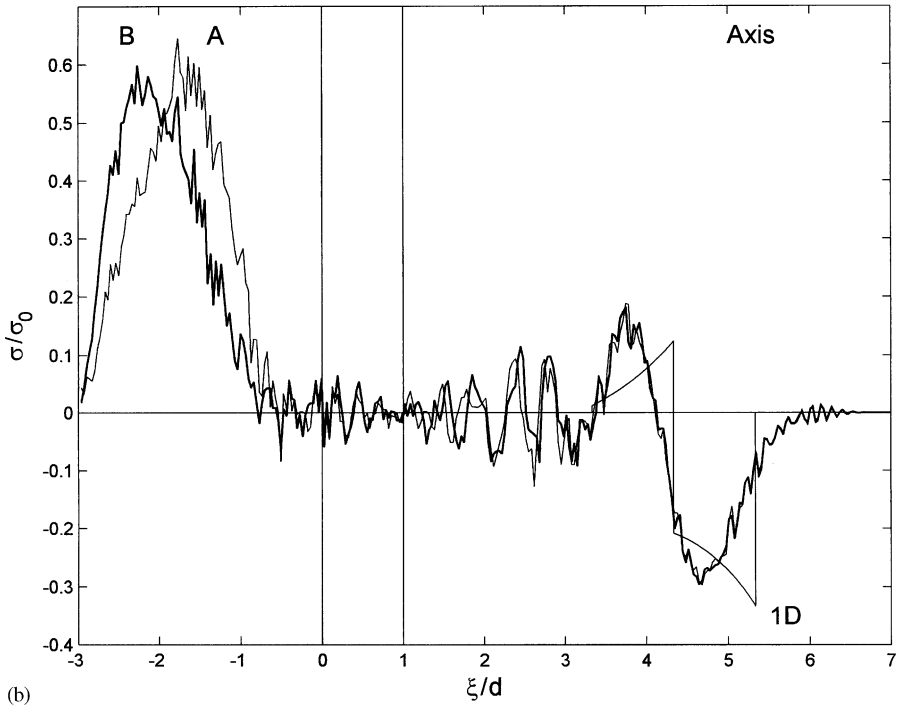

(b)

Figure 7. 3-D and 1-D distributions of axial normal stress at time $t = 5.33d$ in bars with transitions A and B. Ends of transition indicated by vertical lines. Duration of input pressure pulse $\lambda = d$. Coarse mesh. (a) Surface. (b) Axis.

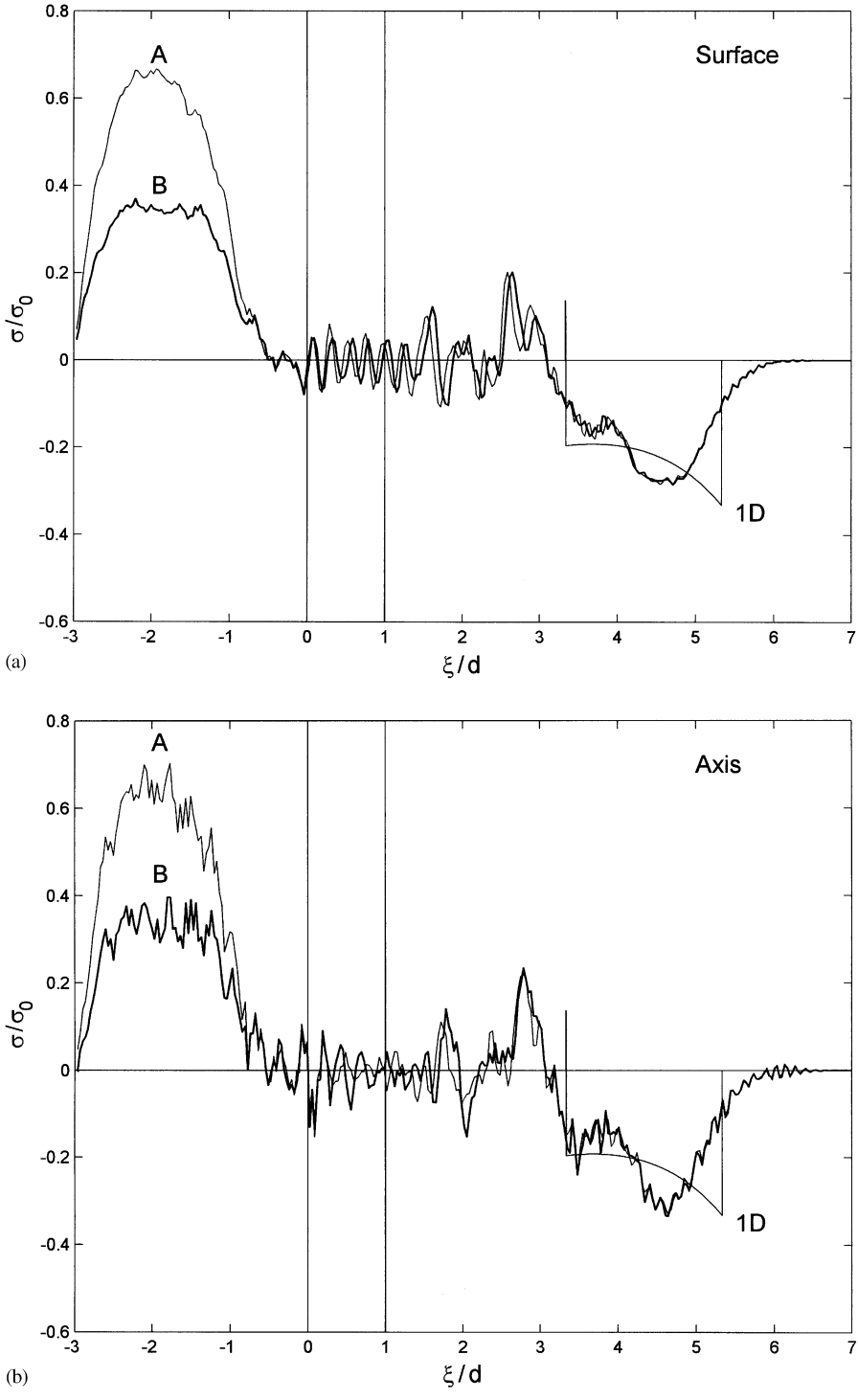

Figure 8. 3-D and 1-D distributions of axial normal stress at time $t = 5.33d$ in bars with transitions A and B. Ends of transition indicated by vertical lines. Duration of input pressure pulse $\lambda = 2d$. Coarse mesh. (a) Surface. (b) Axis.

the leading parts of the 3-D transmitted waves have propagated to $\xi \approx 6d$, thus without reaching the free output ends $\xi = 7d$. At this time, the fronts of the 1-D reflected waves have first undergone free-end reflection with sign reversal at the input ends $\xi = -3d$ and then advanced to $\xi = -0{\cdot}67d$ in the input segments. The leading parts of the doubly reflected 3-D waves have propagated to the proximity of the input end $\xi \approx 0$ of the transition. Figures 6–8 also show the leading parts of the 1-D transmitted waves. In the input segments, Figures 4–8 show the doubly reflected 3-D waves overlapped by the tails of the primary reflected waves.

Figures 4(a)–8(a) show that on the bar surfaces, the 3-D stress distributions are relatively smooth within the leading parts of the reflected and transmitted waves, while within the transitions and the tails of the transmitted waves, they are oscillatory. Figures 4(b)–8(b) show that on the bar axes, the oscillatory character of the stress distributions is more pronounced, especially for the shortest incident wave. This difference in behaviour, on the surface and on the axis, is believed to be explained by the increase in effective axial stiffness of the material near the axis due to the confinement by the surrounding material.

Figures 4 and 5 show, for the incident wave with duration $\lambda = 0{\cdot}5d$, that there is a very good agreement between the results obtained with the fine and the coarse meshes where the stress distributions are smooth, that is, on the bar surfaces along the leading main parts of the reflected and transmitted waves. On the axes, along these parts of the waves, there is a good general agreement between the results obtained with the two meshes. The differences in details are associated with the high-frequency oscillations on the axes. These differences are mainly due to the richer presence of high frequencies with the finer mesh. Along the tails of the transmitted waves, and within the transitions, there are oscillations on the bar surfaces and axes with wavelength $\approx 0{\cdot}37D_{OUT}$. These oscillations with relatively high frequency behind the main transmitted waves are believed to be due to dispersion of geometrical as well as numerical origin. This explains the phase differences between the oscillations along the tails for the two meshes. For the leading main parts of the reflected and transmitted waves, and for the purpose here, the results obtained with both meshes are considered to be satisfactory.

Figure 6 shows, for $\lambda = 0{\cdot}5d$, that the leading parts of the 3-D waves transmitted through transitions A and B are in excellent agreement on the surfaces and in good agreement on the axes over a length of about $3d = 6\lambda$. In the tail behind, there is a fair agreement apart from the phase discrepancies. Similar remarks are valid for the results shown in Figures 7 and 8, which were obtained for incident waves with $\lambda = d$ and $2d$, respectively. Altogether, Figures 6–8 show that transitions A and B are transmission equivalent with good approximation. This result is significant as conditions had been chosen such that (i) these transitions are significantly different from each other and (ii) 3-D effects are significant (if transitions A and B were nearly the same or conditions were nearly 1-D, the result would have been trivial).

The significant difference between the two bar transitions is confirmed by the distributions of stress in the input segments in Figures 6–8 which show that transitions A and B have significantly different reflection properties. The significance of 3-D effects is also confirmed in the same figures in two different ways. Firstly, there is a pronounced disagreement between the 3-D and the 1-D waves transmitted through either transition A or B (a disagreement which was aimed at). Secondly, there is a clear difference between the 3-D stress distributions on the surface and on the axis which does not exist in the 1-D context.

It is concluded that smooth and significantly different elastic bar transitions which are transmission equivalent in a 1-D context may retain this property with good approximation under 3-D conditions, well beyond those under which 1-D theory can be used for prediction

of wave shapes. This extends the domain of potential applications in areas such as percussive drilling correspondingly.

ACKNOWLEDGMENTS

The authors would like to thank AB Sandvik Tamrock Tools and the Grant Agency of the Ministry of Education of the Czech Republic INFRA2, LB 98202, for their economical support.

REFERENCES

1. B. LUNDBERG 1993 in *Comprehensive Rock Engineering*, Vol. 4 (J. A. Hudson, editor), 137–154. Oxford: Pergamon Press. Computer modelling and simulation of percussive drilling of rock.
2. H. KOLSKY 1963 *Stress Waves in Solids*. New York: Dover Publications, Inc.
3. L. H. DONNEL 1930 *Transactions of the American Society of Mechanical Engineers* **52**, 153–167. Longitudinal wave transmission and impact.
4. L.-E. ANDERSSON and B. LUNDBERG 1984 *Wave Motion* **6**, 389–406. Some fundamental transmission properties of impedance transitions.
5. B. LUNDBERG, R. GUPTA and L.-E. ANDERSSON 1979 *Wave Motion* **1**, 193–200. Optimum transmission of elastic waves through joints.
6. R. GUPTA 1982 *Wave Motion* **4**, 75–83. Optimum design of wave transmitting joints.
7. H. KONSTANTY and F. SANTOSA 1995 *Wave Motion* **21**, 291–309. Optimal design of minimally reflective coatings.
8. T. NYGREN, L.-E. ANDERSSON and B. LUNDBERG 1999 *Wave Motion* **29**, 223–244. Optimization of elastic junctions with regard to transmission of wave energy.
9. M. MAO and D. RADER 1970 *International Journal of Solids and Structures* **6**, 519–538. Longitudinal pulse propagation in nonuniform elastic and viscoelastic bars.
10. T. NYGREN, L.-E. ANDERSSON and B. LUNDBERG 1996 *European Journal of Mechanics A/Solids* **15**, 29–49. Optimum transmission of extensional waves through a non-uniform viscoelastic junction between elastic bars.
11. T. NYGREN, L.-E. ANDERSSON and B. LUNDBERG 1999 *Wave Motion* **30**, 143–158. Synthesis of elastic junctions with wave transmission properties of a given junction.
12. T. NYGREN, B. LUNDBERG and L.-E. ANDERSSON 1997 *Journal of Sound and Vibration* **199**, 323–336. Dissipation of energy in a viscoelastic junction between elastic bars: dependence of transmission direction.
13. B. R. MACE 1992 *Journal of Sound and Vibration* **155**, 375–381. Reciprocity, conservation of energy and some properties of reflection and transmission coefficients.
14. J. F. ALLARD, D. LAFARGE, B. BROUARD and W. LAURIKS 1993 *Wave Motion* **17**, 329–335. Reciprocity and antireciprocity in sound transmission through layered materials including elastic and porous media.
15. C. HOESCHL, M. OKROUHLIK, J. CERV and J. BENES 1994 in *Mechanics of contact impact* (M. Okrouhlik, editor); *Applied Mechanics Reviews* **47**, 77–99. Analytical, computational and experimental investigations on stress wave propagation.
16. R. BEPTA and M. OKROUHLIK 1986 *Institute of Thermomechanics Report Z* 998/86, *Prague, Czech Republic*. Dispersive properties of rectangular and square elements for 2D region.
17. M. OKROUHLIK and C. HOESCHL 1993 *Computers and Structures* **49**(5), 779–795. A contribution to the study of dispersive properties of one-dimensional Lagrangian and Hermitian elements.